Journal of Materials Chemistry A

PAPER

View Article Online
View Journal | View Issue

Cite this: J. Mater. Chem. A, 2019, 7, 26456

Robust, sustainable and multifunctional nanofibers with smart switchability for water-in-oil and oil-in-water emulsion separation and liquid marble preparation†

Mohammad Arshadi, Morteza Azizi, Hamid Souzandeh, Chen Tan, Seyed Mohammad Davachi and Alireza Abbaspourrad *

Various membranes have been developed for the separation of oil/water mixtures; however, their fabrication requires toxic reagents, multiple processing steps, and advanced technologies. Nature not only precisely generates unique materials but also provides tremendous examples in the environment that can be used as inspiration for the development and creation of smart and green materials. In this study, we prepare multifunctional nanobiofibers (NBFs) from grape seeds by a one-pot reaction using green solvents that, when made into a smart layer, can switch between a state of underwater superoleophobic wetting to a state of underoil superhydrophobicity and back without any external stimuli. The several μm length and 50 nm width NBFs exhibit robust stability and provide a porous NBF layer, suggesting their potential for the simultaneous separation of various surfactant-stabilized water-in-oil and oil-in-water emulsions while showing high dye adsorption from water (100% for methylene blue). Furthermore, by rolling water droplets on the surface of NBF powder, an effective microreactor, known as a liquid marble, is prepared for the first time using a bio-originated, superamphiphilic material in air, rather than hydrophilic or hydrophobic materials, and it can be used to remove dye within 30 s. Moreover, based on the ability of NBFs to encapsulate a high volume of water (120 μL), we demonstrate another application of the NBF powder as an additive to soil for maintaining soil moisture under arid conditions, allowing us to successfully demonstrate the growth of a lentil seed. This multi-functional, low-cost, and green NBF material shows excellent sustainability and mechanical/chemical stability for multiple promising environmental remediation applications.

Received 18th September 2019
Accepted 31st October 2019

DOI: 10.1039/c9ta10320a

rsc.li/materials-a

1. Introduction

The amount of energy consumed for the separation of chemicals is approaching ~10–15% of the world's total energy consumed per year.[1] Furthermore, in recent years oil contamination from frequent spills and increasingly oily industrial sewage has become one of the most important issues that threaten the environment and water resources.

Several traditional methods like air flotation, flocculation, oil-absorption, gravity separation combined with skimming, and coagulation are currently being used for oil/water separation and suffer from low separation performance, complicated separation steps and high energy consumption, which make them unable to separate tiny water and oil droplets from water-in-oil and oil-in-water emulsions in one step.[2,3] Separation technologies that rely on filtration-based systems can purify oil/water mixtures by efficient, green, and low-cost energy processes.[4] Synthetic filters and membranes with outstanding wettability known as superhydrophilic–superoleophilic (SHP–SOP) membranes are used extensively to separate oil–water mixtures and emulsions in various settings, including gasoline and fuel purification and oil spill clean-up.[5] However, most materials and surfaces that have superhydrophobic properties in air can be easily deactivated or fouled with oil. Therefore, the process of overhauling and cleaning such membranes requires an enormous amount of time, money, and energy.[6] Additionally, as the density of water is higher than that of oil, the water molecules can form a barrier across horizontally oriented SHP–SOP membranes, which can suppress oil permeation and decrease the flux of the system.

Underwater separation of oil-in-water emulsions can now be accomplished with a green, potent, cost effective and reliable method. Recently, inspired by the advantages of the superoleophobic properties of fish scales and other bio-originated materials, researchers have produced biomimicry-based anti-

Department of Food Science, College of Agriculture and Life Sciences, Cornell University, 243 Stocking Hall, Ithaca, NY 14853, USA. E-mail: Alireza@cornell.edu

† Electronic supplementary information (ESI) available. See DOI: 10.1039/c9ta10320a

oil-fouling surfaces.[7,8] In fact, the existence of a micro/nanoscale topographical framework on the surface of fish scales provides high roughness and the ability to adsorb water molecules and form a thin layer of water on their surface, which suppresses the attachment and fouling of oils on the surface. Unfortunately, due to the higher surface tension of water than of oils and the extremely low surface tension of the bioinspired oil-repellent surface and membrane, this type of material mostly prefers to repel water as well. Indeed, there have been a few studies on the preparation of sustainable superhydrophilic/underwater superoleophobic membranes with water and oil contact angles less than 5° and greater than 150°, respectively.[2,3,9–15] Moreover, the preparation of surfaces featuring underoil superhydrophobic and underwater superoleophobic properties often has disadvantages including (i) complicated synthesis steps, (ii) expensive processes, (iii) laborious procedures, (iv) the use of toxic and antagonistic chemical reagents, and (v) the necessity of complex facilities, all of which challenge the implementation of the hydrophobic/hydrophilic materials for oil/water separation.[16–21]

As an alternative, we report a smart SHP–SOP filter made from grape seeds that is simple to fabricate, green, low-cost, and mass-producible, demonstrating both underwater superoleophobic and underoil superhydrophobic properties. Grape seeds are a natural and sustainable biomass source and are considered a waste material by the wine and grape juice industries. In fact, the vineyards have to pay a grape pomace disposal fee; therefore, the precursor material for preparation of the NBF membrane has a very low-price (∼2–3 cents per kg) for a large scale.[22–24] Additionally, grape seeds do not leach harmful compounds into water, making it a safe raw material for use in water treatment applications. We designed a simple and sustainable activation process that turns grape seeds into nanobiofibers (NBFs) without the use of carbonization or any toxic organic reagents or solvents. Instead, we simply treat ground dried grape seeds (*i.e.*, grape pomace, derived directly from winery-based biomass waste) with sodium hydroxide (NaOH) in a one-pot reaction, from which we are able to easily obtain high purity NBFs as a value-added product. The individual NBFs are short and have a uniform structure and can be stuck to and packed on each other, forming a porous and smart substrate (membrane). The produced membrane demonstrates remarkable wettability properties and can be easily switched from an underwater superoleophobic membrane to an underoil superhydrophobic filter. This happens as the continuous phase of emulsion changes from water to oil, making the membrane a strong candidate for the purification of oil/water emulsions. Furthermore, this system features the unique capability to separate both oil-in-water and water-in-oil emulsions without any pre- or post-treatment while still maintaining its high permeability and antifouling ability.

Additionally, we extend the application of this low-cost and green NBF powder to encapsulate water droplets and prepare marble liquid using a bio-originated superamphiphilic material in air for the first-time, instead of hydrophilic or hydrophobic materials,[25–29] which acts like a shell to stabilize a high volume of water in a droplet (120 μL) in air. Furthermore, based on this unique property, we demonstrate the ability of the NBF material to serve as a soil additive to enhance moisture retention and study its ability to promote the growth of lentil seeds under otherwise dry conditions. Our findings indicate that in addition to the separation characteristics, NBFs can also serve as a physical barrier in suppressing the evaporation of water to retain soil moisture. The fabrication of these NBFs is simple, inexpensive, scalable, and green, enabling the production of a novel multifunctional material.

2. Experimental section

2.1. Materials

The grape pomace was collected from the Cornell Wine Lab at Cornell University in Ithaca, New York. NaOH (98%), kerosene, vacuum pump oil, hexane, Span 80, and all solvents were purchased from Sigma-Aldrich. Corn oil was obtained from a local grocery store. All aqueous solutions were synthesized using distilled water.

2.2. Synthesis of NBFs

The grape seeds were separated by hand from the stems and skins of the grape pomace. Once the seeds were separated and rinsed with distilled water, they were dried overnight (∼16 hours) at 77 °C. The dried biomaterial was then ground using a mortar and pestle and sieved to a 20 mesh, or 841 μm particle, size. Then 20 grams of this separated grape seed was added to 300 mL of a 0.1 M NaOH solution and stirred on a stir plate for 2 h at 100 °C to obtain the NBFs. The resulting NBFs were filtered and rinsed with water, ethanol, and acetone, and dried overnight at 77 °C. The final NBF material was stored at room temperature in a 50 mL plastic vial.

2.3. Preparation of NBF membrane

The NBFs (1 g) were poured onto stainless-steel mesh no. 100 with a diameter of 1 cm and a fixed bed of the NBFs was prepared by placing another stainless-steel mesh on top to stabilize the NBF bed in position. The density (ρ_{layer}) and the porosity (ε_{layer}) of the NBF layer, the density of the NBF powder (ρ_{NBF}), and the average pore radius (r_p) of the prepared NBF membrane were 0.615 g cm^{-3}, 91.8%, 0.67 g cm^{-3}, and 2.7 μm, respectively, based on the corresponding equations in Table S1.† The average pore size (2.7 μm) was obtained using ImageJ software.

2.4. Characterization

The morphology and structure of the grape seeds and the obtained NBFs were studied using a Zeiss Gemini 500 field emission scanning electron microscope (FE-SEM) equipped with an energy dispersive X-ray spectrometer (EDX) and a transmission electron microscope (TEM), FEI T12 Spirit TEM STEM, operated at 120 kV. X-ray photoelectron spectroscopy (XPS) was performed using a Surface Science Instruments SSX-100 XPS system at an operating pressure of ∼2× 10^{-9} torr. The thermal behavior and stability were monitored by thermogravimetric analysis (TGA Q500, TA Instruments, New Castle, DE, USA) and

differential scanning calorimetry (DSC Q2000 TA Instruments, New Castle, DE, USA). The attenuated total reflectance-Fourier-transform infrared (ATR-FTIR) spectra were recorded between 400 and 4000 cm^{-1} with a resolution of 4 cm^{-1} using an IRAffinity-1S spectrometer equipped with a single-reflection ATR accessory (Shimadzu Corp., Kyoto, Japan). The contact angle was determined using a contact angle machine (model190CA, Ramé- Hart Instrument, Netcong, NJ). Dynamic light scattering (DLS) of the emulsions was recorded at 25 °C using a zeta-sizer (Nano-ZS90, Malvern Instrument Ltd., UK) with a scattering angle of 90° and a He/Ne laser ($\lambda = 633$). The amount of water in the oil filtered through the NBF membrane was calculated using a Karl Fischer Titrator. The pore size of the NBF membrane was obtained from the SEM images using ImageJ software. The 3D image of the NBF membrane was scanned using a Keyence VK-X260 laser-scanning confocal microscope (Keyence Corporation of America, USA). A UV-2600 spectrophotometer (Shimadzu, Japan) was used to monitor the concentration of oil and methylene blue in water. The oil separation efficiency of the NBF was monitored by measuring the hexane concentration in emulsion and in filtrated water with the UV-vis absorption spectrometer (red O was used to dye hexane).

2.5. Separation of water-in-oil emulsions

To synthesize the surfactant stabilized water-in-oil emulsion, four types of oils (hexane, kerosene, vacuum pump oil, and corn oil) were mechanically mixed with 0.1 g of span 80 for 10 min, after which water was slowly added to the oil mixtures with continuous shaking to achieve a volume ratio of 1(water)/50(oil) ml/ml. Then the whole mixture was sonicated at a power of 450 W for 1 h and vortexed for more than 3 h at 25 °C to generate a stable milky solution of a water-in-oil emulsion. The same procedure was used to prepare surfactant-free emulsions without the use of Span-80. The as-prepared emulsions were able to pass through the NBF membrane sandwiched between the two stainless steel meshes simply by gravity, with the transparent oils collected into a volumetric glass container. The height of the water-in-oil emulsion separation glass column was fixed at 73 cm ($\Delta P = 7.3$ kPa) and the flux was monitored for each oil emulsion. The used NBFs were regenerated by flushing them with ethanol twice and drying at 80 °C in a vacuum oven for 3 h.

2.6. Separation of the oil-in-water emulsion

For the oil-in-water emulsion, 0.2 g span 80 was added into 100 mL water, and then 2 mL hexane was added to the mixture. The mixture was sonicated at a power of 450 W for 1 h and vortexed for more than 1 h at 25 °C to generate a stable milky solution of an oil-in-water emulsion. The same procedure was used to prepare surfactant-free emulsions without the use of Span-80. The as-prepared emulsion was able to pass through the NBF membrane sandwiched between the two stainless steel meshes simply by gravity, with the transparent water collected into a volumetric glass container. The height of the oil-in-water emulsion separation glass column was fixed at 73 cm ($\Delta P = 7.3$ kPa) and the flux was monitored. The used NBFs were regenerated twenty times by flushing them with ethanol and water and drying at 80 °C in a vacuum oven for 3 h.

2.7. Preparation of liquid marble

A bed of NBF powder was prepared in a Petri dish with 2–3 mm thickness and then sessile water droplets with various volumes, ranging from 5 to 120 μL, were gently rolled on the bed of NBFs and within 10 seconds, the water droplets were completely encapsulated to generate liquid marbles.

2.8. Soil growth studies and plant measurement

6 g of different soil treatments (loam) and several lentil seeds (*Lens culinaris*), purchased from a local grocery store, were added to separate glass vessels (diameter of 1.5 cm and volume of 10 mL). The five soil treatments used were (T1) 100% soil (control), (T2) 60% NBFs (top layer) and 40% soil (bottom layer), (T3) 50% NBFs (top layer) and 50% soil (bottom layer) and (T4) 50% NBF mixed with 50% soil to study the effect of the added NBFs on the growth of the lentil seeds. The lentil seeds were incubated for 20 days in the glass vessels illuminated with cool-white fluorescent light at a temperature of 27 °C. Initially 3 mL water was added to all the vessels. Throughout the incubation period, the glass vessels were manually watered with 1 mL every 4 days to maintain moist conditions to grow the seeds. Lentil growth was measured at the end of the test period. Each treatment test was repeated three times. Soil, lentil seeds and plants were collected from each vessel after 20 days and the soil and NBFs were gently removed by washing with water and the height of the plant and roots was measured using a digital ruler (Neiko 01407A).

3. Results and discussion

To prepare the raw material for processing, we ground the pre-separated grape seeds into a fine powder and sieved the material to a particle size less than 50 μm (Fig. 1). We then removed impurities, pectin, lipids, lignin, contaminants, and pigments from the surface of the grape seed powder by stirring the raw material in a NaOH solution, followed by filtration and drying to obtain the NBFs (Fig. 1A–D).[30–33] When comparing the ATR-FTIR spectrum of the grape seeds with that of NBFs significant differences were found of which the absorption bands at 783 cm^{-1} ($CH_{2\ rocking}$ of phenolics), 1317 cm^{-1} ($CH_{2\ scissoring}$ of polysaccharides, pectins), 1438 cm^{-1} (C–$C_{aromatic}$ of phenolics), 1605 cm^{-1} (COO^- and C=$C_{aromatic}$ of pectins and phenolics), 1742 cm^{-1} (C=O_{ester} of polyesters, pectins and lignins), 2852–2923 cm^{-1} ($CH_{2\ aliphatic}$ of lignins and lipids) and 3003 cm^{-1} (= C–H of aromatic ring) disappeared on the NBF surface and those in the chemically stable backbone of the NBFs remained (Fig. S1†).[34–37] It is noteworthy that NBFs exhibit a very small and broad peak at 3300 cm^{-1} belonging to the –OH stretching vibration, compared to the commercial cellulose nanofibers and crude grape seeds.[38] This peak shows that the NBFs have a small amount of water, leading to a lighter weight and more active carbon framework for further interactions. Moreover, the

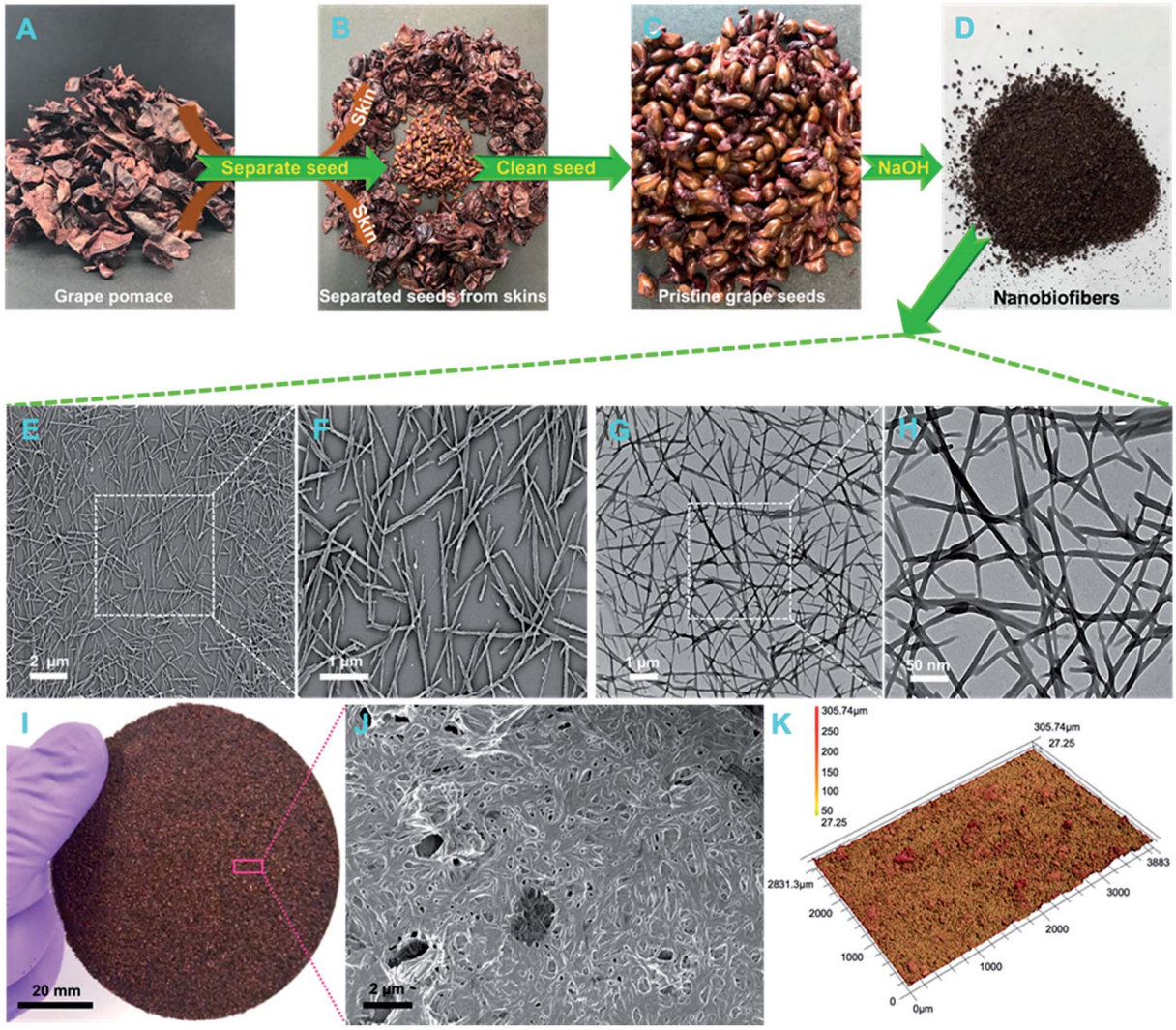

Fig. 1 (A–C) Schematic illustration of the preparation of NBFs from grape pomace. (D) Optical, (E and F) SEM, and (G and H) TEM images of the NBF powder, (I) photograph of a NBF membrane, (J) SEM image of the NBF membrane, and (K) 3D image of the NBF membrane.

disappearance of the peaks at 1743 and 1521 cm^{-1} are attributed to the acetyl and uronic ester linkage of carboxylic groups of the ferulic and *p*-coumaric acids of lignin or to the hemicelluloses and aromatic rings of lignin, respectively.[39] This confirms that the active available material in the structure of NBFs is, most likely, the cellulose structure.

We also studied the thermal stability of the grape seeds and the NBFs using TGA and DSC characterization (Fig. S2†). As shown in Fig. S2A,† TGA and DTGA data revealed moisture evaporation at low temperatures—from 25 to 100 °C—at which NBFs absorbed more moisture than the grape seed samples (potentially due to the removal of impurities like lipids from the NBFs' oxygen framework).[30–32,40,41] Both the grape seed and NBF samples showed a rapid change at ~220–380 °C due to the degradation of their organic compounds. The grape seed sample shows three small steps, shown in DTGA data as three small peaks at 408, 476 and 610 °C that can be related to the oxidation and breakdown of charred residues.[40] The only observed degradation is caused by pyrolysis of the carbon framework of the NBFs.[31] The slightly lower intensity of the NBF DTGA peak (at 330 °C) compared to that of grape seeds (346 °C) is due to the faster heat transfer of the cellulose in NBFs. Furthermore, NBF data also show higher ash content because of the NaOH washing procedure and possible sodium interactions that has been further confirmed by SEM-EDX.[42]

The DSC curves (Fig. S2B†) demonstrate a very low glass transition temperature (T_g) for both samples. NBFs exhibit a lower T_g (−36 °C) compared to grape seeds (−31 °C), probably due to the removal of impurities and lipids. The very low T_g shows that these cellulose-based materials can be very effective for low temperature applications. The DSC curves of NBFs show lower thermal stability compared to grape seeds due to changes in the structure or degradation at 170 °C. Meanwhile, the grape seeds are completely stable even at higher temperatures. There are two likely reasons for this behavior. First, the higher surface area of NBFs compared to the grape seeds could increase the thermal conductivity and, therefore, the rate of heat transfer. The same property has been reported for cellulose

nanocrystals.[43] Second, cellulose will decompose to levoglucosan around 180 °C which is then gasified efficiently at 300 °C. This may explain the sudden change in weight appearing in the DSC curve of NBFs. As there is no lipid or other protection, this change is more visible in NBFs and this decomposition in grape seeds might happen at higher temperatures.[42]

Compared to those of the pristine grape seeds (Fig. S3†), the SEM and TEM images as well as the SEM-EDX data of the treated grape seeds showed pure nanofiber structures that were 0.5–3 μm long and 10–15 nm wide, which indicated that most of the impurities were removed from the surface of the grape seeds, leaving pure NBFs behind with high mechanical stability after long-term (one month) exposure in either acidic (pH = 2) or basic (pH = 13) solutions under mechanical stirring conditions (Fig. 1E–H and S4†). Compared with the reported sizes for commercial cellulose nanofibers, NBFs have a short, unique, uniform, and unbranched individual nanofiber structure, providing more advantages to NBFs.[38] Moreover, the removal of lipids, pectin, and other impurities is further confirmed by SEM-EDX (Table S2†). The grape seeds have P, K, Si and Mg elements. The NBF EDX results did not show any of these elements. The NBF membrane was obtained by sandwiching NBF layers between two stainless steel meshes. A centimeter-sized NBF membrane is shown in Fig. 1I. The SEM image of the NBF membrane shows a microscale, porous framework resulting from the aggregation and stacking of NBFs (Fig. 1J). Furthermore, laser scanning confocal microscopy was used to observe the NBF membrane's 3D topographical framework, in which an average surface roughness of the NBF membrane of 12.2 μm was observed (Fig. 1K).

To assess the surface wettability of the NBF membrane, we measured the water and oil contact angles in air (Fig. 2A and B). Both water and oil droplets (2 μL) penetrate and diffuse within 130 ms on the surface of the NBF membrane, resulting in

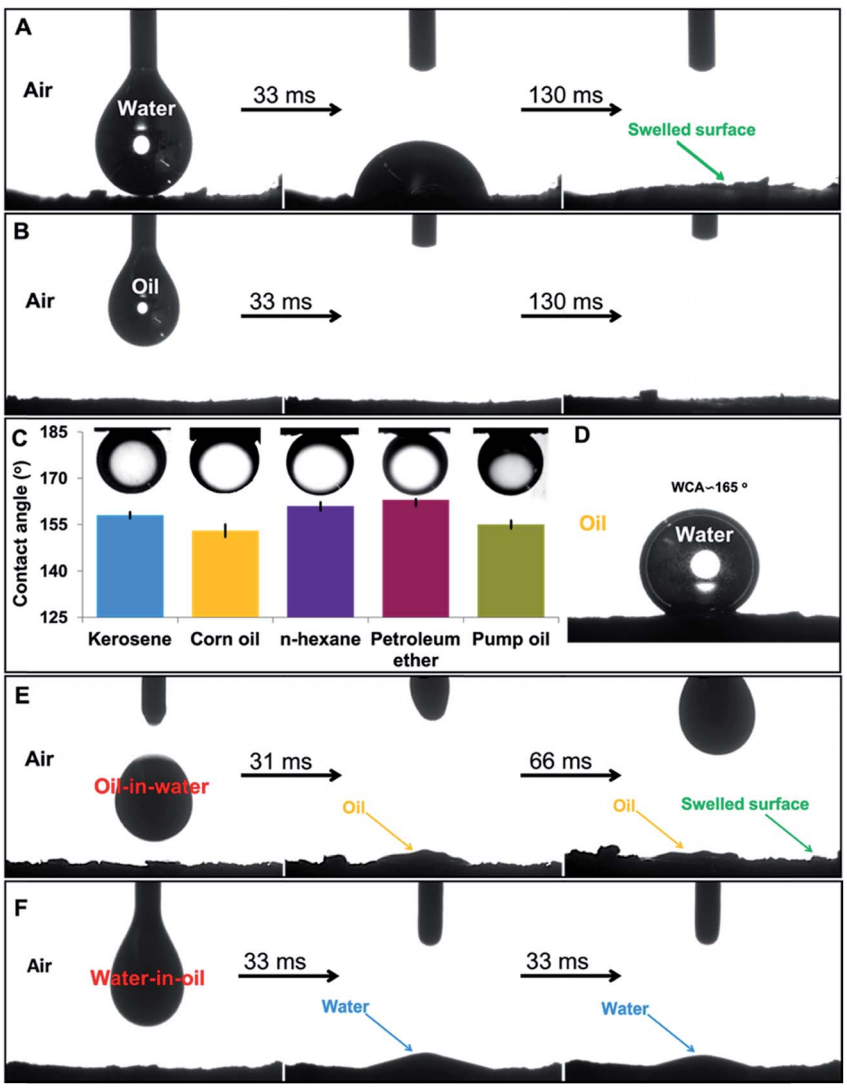

Fig. 2 (A and B) Photographs of the dynamic measurement results of water and oil permeation on the surface of the NBF membrane. (C) Variation of the different underwater oil contact angles. (D) The water contact angle underoil of the NBF membrane. (E) The oil-in-water and (F) water-in-oil permeation on the surface of the NBF membrane.

a contact angle of nearly 0° in both cases (Movies S1 and S2†). When water is dropped on the NBF membrane, the membrane's surface adsorbs the water and starts to swell within a millisecond (Fig. 2A). Indeed, the NBF membrane is superamphiphilic in air because of its large surface energy due to the high concentration of hydroxyl groups on the surface of the NBFs.[44] Furthermore, the superhydrophilic NBF membrane shows unique underwater superoleophobicity, with an oil contact angle as high as 153° or higher when different types of oil (*e.g.*, kerosene, corn oil, pump oil, hexane, and petroleum ether) were used (Fig. 2C). This behavior suggested the membrane's potential for oil/water emulsion separation underwater.[45] Due to the material's high surface energy, the high content of water molecules trapped on the surface of the NBFs and the rough micro/nanostructures of the NBFs the contact area of the oil droplets with the surface of the membrane decreases, leading to a unique superoleophobic surface with a large oil contact angle underwater.[9,46–48] However, we also found that the water contact angle of the NBF membrane under oil was 165°, which demonstrates the superhydrophobicity of the NBF membrane (Fig. 2D, Movie S3†). In this case underoil, the trapped layer of oil molecules on the surface of the membrane appears to act as a repulsive liquid phase that suppresses the penetration of water through the membrane surface, resulting in underoil superhydrophobicity.

To evaluate the surface wettability of the NBF membrane in detail, we also studied the wetting behavior and dynamic interaction of the oil-in-water emulsion and water-in-oil emulsion droplets on the membrane. When a droplet of the oil-in-water emulsion comes into contact with the surface of the membrane, water molecules penetrate through the nanostructure of the membrane within 31 ms and the wetted membrane starts to swell within 66 ms and consequently the oil particles remain and aggregate on the surface of the membrane (Fig. 2E, Movie S4†). The reverse situation occurs in the case of dropping a water-in-oil emulsion on the surface of the membrane after which the oil immediately passes through the membrane within 33 ms and the water droplets are blocked on the surface of the membrane (Fig. 2F, Movie S5†). As a result, we conclude that whatever the continuous or dispersed phase (oil or water) the membrane is able to separate various emulsions. When the continuous phase is water in an oil-in-water emulsion, the NBF membrane will be superhydrophilic and under-water superoleophobic, enabling the filtration of the oil from the water phase. However, in a water-in-oil emulsion the continuous oil phase changes the response of the NBF membrane to be superoleophilic and underoil superhydrophobic, accelerating the penetration of oil and the separation of water.

These results show how we are able to successfully prepare a green, low-cost, smart, and switchable membrane at room temperature from biomass (grape pomace) using a simple process without the use of any toxic or chemically hazardous reagents. As a result, we anticipate that our unique synthesis method could be used to fabricate membranes in developing countries for the separation of oil/water and water/oil emulsions.

We also studied the functionality of our NBF membrane for the separation of different types of oils from surfactant-free water/oil mixtures and surfactant-stabilized water-in-oil emulsions. To investigate the filtration performance of the NBF membrane, pump oil, corn oil, kerosene, hexane, and petroleum ether were selected to make an emulsion with or without stabilization using Span 80 as the surfactant. Fig. 3A shows the oil purity in the filtrate after passing different stabilized and non-stabilized water-in-oil emulsions through the NBF membrane. The NBF membrane showed significant oil purification performance (99.9%) for all types of oil with or without the use of surfactant. We also found that for Span 80-free samples, the oil purity in the filtrate stayed between 99.95% and 100% for all types of oils. On the other hand, for surfactant-stabilized materials, the oil purity slightly decreased, with the NBF membrane displaying the highest and lowest purity for pump oil (99.96%) and hexane (99.87%), respectively.

Fig. 3B shows the water content in the filtrate after passing different stabilized/non-stabilized oils through the NBF membrane. The water content is less than 10 ppm for the surfactant-free samples, which confirms the results described above. Meanwhile, the lowest water contents of 3 and 5 ppm were achieved when vacuum pump oil and corn oil were used, respectively. Likewise, similar to the phenomenon observed before, the water content in the filtrate for the water-in-hexane emulsion with span 80 was the highest (10.3 ppm). As a result, we found that with the use of the surfactant Span 80, the water content in the pump oil emulsion increased from 3 to 8 ppm while for hexane it went up from 10 to 26.4 ppm. We also investigated the permeability of the NBF membrane to evaluate the filtrate flux of the water-in-oil emulsion separation process (Table S1† and Fig. 3C). Our results indicated that the permeate flux of the membrane did not depend significantly on whether or not surfactant was used in the different water-in-oil emulsions explored. However, the flux is heavily dependent on the oil's viscosity. Consequently, the fluxes for the pump oil and corn oil (312 ± 21 and 428 ± 30 L m^{-2} h^{-1}, respectively) were essentially far lower than those of the less viscous hexane and petroleum ether emulsions, which exhibited flux values of 4844 ± 127 and 4501 ± 87.5 L m^{-2} h^{-1}, respectively (Fig. 3C). We also note that compared to the permeation properties of previously reported superhydrophilic membranes,[3,18,49] the flux results shown here demonstrate the extraordinary permeability of the NBF membrane without the use of any external pressure.

We believe that the difference in oil purity among the various water-in-oil emulsions used directly depends on their viscosity. As hexane has the lowest viscosity amongst these oils, the flux through the membrane is higher and the passing emulsion has less time to interact with NBFs. On the other hand, pump oil and corn oil possess higher viscosities and thus have enough time to interact with the membrane, which results in higher filtration performance for these oils. Moreover, the use of a surfactant helps stabilize the smaller water droplets, which makes it harder to filter them from the passing fluid. Therefore, a slight drop in oil purity was seen when using surfactant-stabilized emulsions. However, we note that the oil purity in the filtrate was well over 99.85% for all samples, which is

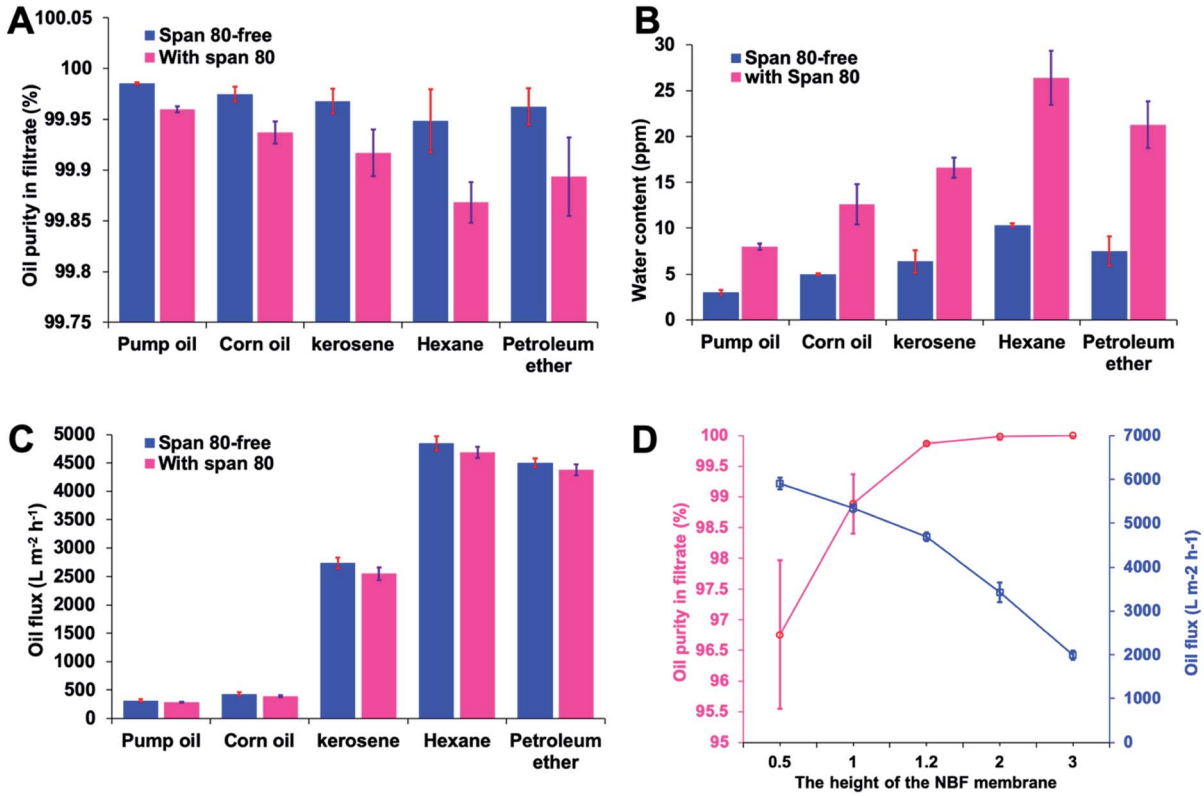

Fig. 3 (A) Separation capabilities of the NBF membrane for span 80-stabilized and span 80-free water/oil emulsions made with different oils. (B) Water content in the filtrates of span 80-stabilized and span 80-free water/oil emulsions. (C) Oil permeation flux of the NBF membrane for span 80-stabilized and span 80-free water/oil emulsions. (D) The effect of the height of the NBF membrane on its separation capability and oil flux for span 80-stabilized water/hexane emulsions.

promising for the use of our very low-cost and sustainable membrane, in comparison to the other reported systems,[2,49,50] on a large scale, especially in resource-limited countries/settings.

In order to investigate the effect of the height of the NBF membrane on its separation capability and oil flux, we chose the Span 80-stabilized water/hexane emulsion sample as a representative. As shown in Fig. 2D, when we increased the bed height of the NBF membrane from 0.5 to 1.2 cm, the oil purity in the filtrate increased from 96.75% to 99.87%. Furthermore, when we increased the bed height further above 1.2 cm, the oil purity of the filtrate reached 100%. This can be attributed to the longer contact time and greater interaction of the emulsion feed with the thicker NBF membrane. On the other hand, after increasing the bed height from 0.5 to 1.2 cm, the oil flux slightly decreased from 5901 to 4687 L m^{-2} h^{-1}, and by further increasing the height to 3 cm, the oil flux drastically decreased to 1993 L m^{-2} h^{-1}. This phenomenon is reasonable since increasing the membrane bed height leads to a higher pressure drop, where the friction forces reduce the flux of a liquid through a column, and consequently the flux drops significantly.[51] We further studied the relation between the emulsion feed flux and the height of the NBF membrane using the Hagen–Poiseuille equation (Table S1†); based on the equation and our results using different oils (Fig. 3C, Movie S6†) and NBF heights (Fig. 3D), we found that the flux displays an inverse proportional correlation with the viscosity of oil and the height of the NBF bed. Therefore, the flux is only affected by the oil viscosity and thickness of the membrane.[52]

Due to the fact that every membrane has a saturation point and is only capable of adsorbing a certain amount of water, we calculated the theoretical value of the separation capacities of various water-in-oil emulsions by the NBF membrane (see Table S1†). To achieve the experimental NBF membrane water adsorption saturation point (m_0) in the emulsion separation process, we considered the first drop of filtrate which turned from transparent to turbid (or the milky color of the pristine emulsion) as an indication of the end of separation and thus the membrane's saturation point. Fig. 4A shows the theoretical and experimental amounts of filtered volumes before saturation of the NBF membrane for different water-in-oil emulsions both with and without Span 80. The NBF membrane exhibited lower separation capacities for the Span 80-stabilized samples (20–32 mL (oil) g^{-1} (NBF membrane)) compared to the Span 80-free (22–36 mL g^{-1}) water-in-oil emulsions. As described earlier, the separation performance of the Span 80-stabilized water-in-oil emulsions was generally lower than that of the span 80-free emulsions because the surfactant leads to smaller stabilized water droplets.[53] Thus, these stable microdroplets of water

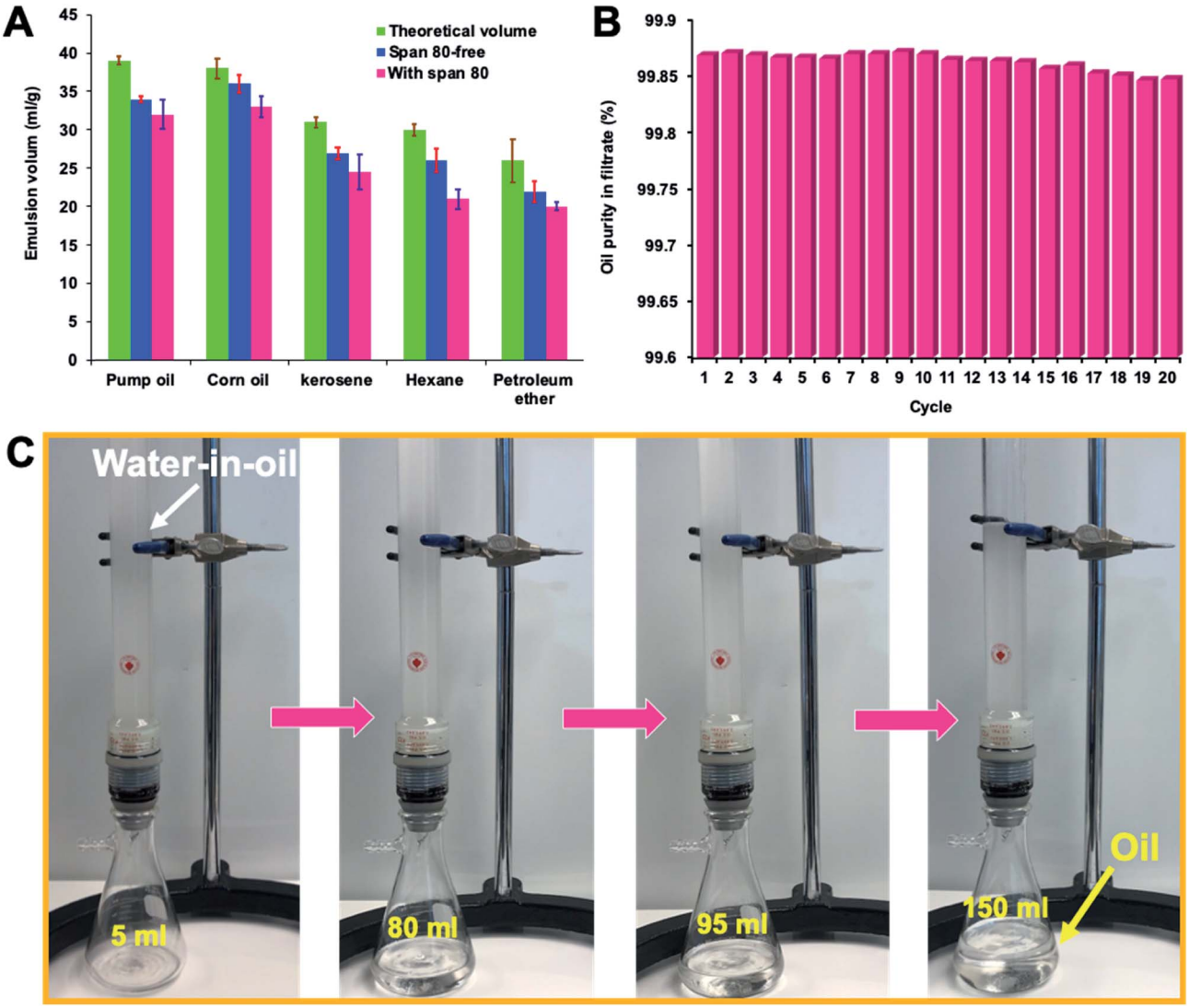

Fig. 4 (A). The theoretical and experimental amount of oil volumes filtered by the NBF membrane for span 80-stabilized and span 80-free water/oil emulsions. (B) The change in oil purity of the Span 80-stabilized water/hexane emulsion filtrate over twenty filtration cycles using the same NBF membrane. (C) Photos illustrating the process of separating the Span 80-stabilized hexane-in-water emulsion using the NBF membrane (height of 1.2 cm).

dispersed in the Span 80-stabilized emulsions do not have enough time to merge and aggregate to form larger droplets compared to those in the Span 80-free samples at the NBF membrane interface.

To be economically viable, separation membranes must be reused multiple times, ideally without significant degradation in performance. To explore the recyclability of our NBF membrane for the separation of water-in-oil emulsions, we used the Span 80-stabilized water-in-hexane sample as a model feed liquid and measured the oil filtrate purity after twenty cycles of filtration (Fig. 4B). After each cycle, the NBF membrane was washed with ethanol and then dried at 75 °C to prepare the filter for the next use. Fig. 4B shows that over twenty cycles, the NBF membrane maintained significantly stable performance, with an oil purity that ranged between 99.85% and 99.87% in the filtrate liquid.

Furthermore, as illustrated in Fig. 4C, the NBF membrane shows excellent mechanical stability and separation efficiency in the separation of water from oil when a long glass tube with a height of 73 cm was installed and the water-in-oil emulsion was poured directly into this homemade system. Based on the intrusion pressure equation (Table S1†), we estimate that the durability of the NBF membrane could last and the membrane could preserve its ability under a high intruding pressure of 7.32 kPa, which is higher than that for most previously reported superhydrophilic membranes,[3,54,55] suggesting that the proposed material should demonstrate excellent performance on a large scale.

We also monitored the water-in-oil emulsions before and after the filtration process using optical microscopy and DLS (Fig. S5†). The water droplet sizes of the hexane and pump oil solutions were smaller than 6 nm, while for corn, petroleum

ether, and kerosene the droplet size was significantly greater at ~1000 nm, which could be due to the difficulty of achieving water droplet dispersions in these oils under the conditions used. Interestingly, no water droplets were dispersed in the filtered solution after passing the feed emulsion through the NBF membrane because the Zetasizer instrument did not yield any particle size which again confirmed the unique and remarkable ability of the membrane in purification of the oil.

To better characterize the switchability of the NBF membrane from superhydrophilicity to superhydrophobicity, we studied the separation of the hexane-in-water emulsion stabilized with Span 80. By pouring the oil-in-water emulsion feed onto the NBF membrane transparent water immediately passed through the membrane while oil was blocked on the membrane's surface, and the performance of the NBF membrane was further confirmed by comparing digital and microscopic images of the dense oil droplets in the emulsion feed, which appeared milky-white, with those of the transparent solution of the filtered water, which featured no droplets (Fig. 5A, Movie S7†). Furthermore, DLS data revealed that only a few 1 nm oil droplets were observed in the purified water after the ultrafast filtration process using the NBF membrane (Fig. 5B).

We also evaluated the chemical stability of the NBF membrane at different pHs using hexane-in-water emulsions made with water that ranged in pH from 2.1 to 11.0 (Fig. 5C). The water permeation flux slightly increased from 1021 L m^{-2} h^{-1} to 1150 L m^{-2} h^{-1} as the pH values increased from 2.1 to 11.0. Additionally, we found that the membrane demonstrated stable oil separation performance, with 100% water filtrate purity for all pH values ranging from 2.1–11.0, suggesting the excellent chemical stability of the membrane under basic and acidic conditions, allowing it to retain its ability to filter water with high purity.

To further evaluate the practical applications of the proposed membrane we measured the permeate flux for both

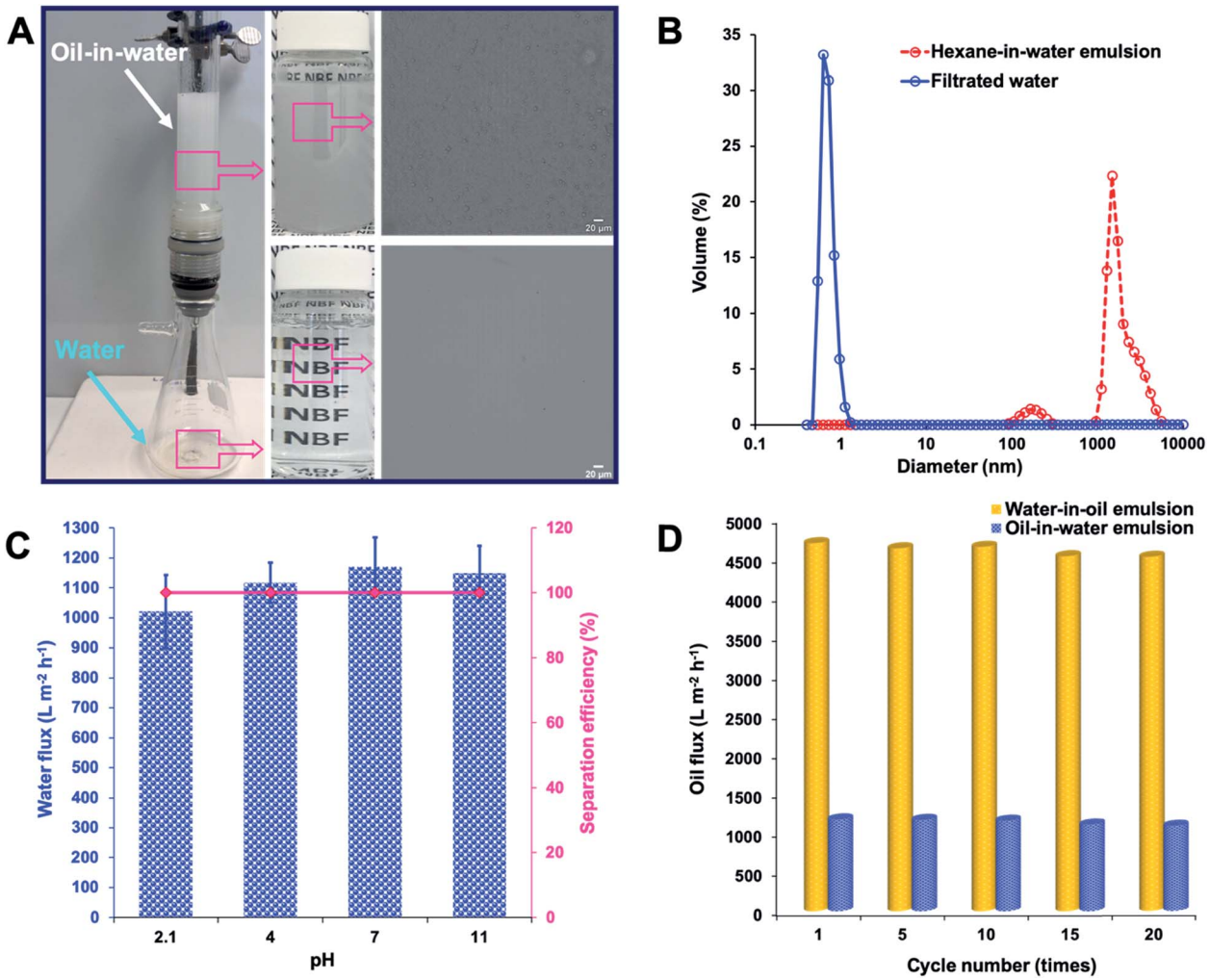

Fig. 5 (A) The purification process using a lab-made filtration unit and microscopy images of a hexane-in-water emulsion stabilized with Span 80 before (top) and after (bottom) separation. (B) Particle size analysis of the Span 80-stabilized hexane-in-water emulsion feed and filtered water. (C) The permeation flux and separation efficiency of the NBF membrane for the Span 80-stabilized hexane-in-water emulsion at different pH values. (D) The permeation flux of the NBF membrane for the Span 80-stabilized water-in-hexane and hexane-in-water emulsions after multiple cycles of filtration.

the water-in-hexane and hexane-in-water emulsions after 20 cycles of the separation process (Fig. 5D). In addition to high water-in-oil and oil-in-water emulsion purification performance of the membrane, we found that the permeability for both emulsions was noticeably unchanged as the number of filtration cycles was increased. This finding suggests that the NBF membrane has excellent antifouling properties, to which the low oil-adhesion and water-adhesion under opposite phase conditions of the NBF membrane substantially contribute. The high purity of the filtrates and the high permeate flux verify the membrane's capability to filter both water-in-oil and oil-in-water emulsions, facilely switching its transport properties upon exposure to these various solutions.

In addition to its excellent and versatile filtration properties, the NBF membrane also displays efficient adsorption towards methylene blue (MB)—a toxic and carcinogenic positively charged dye commonly used in the textile industry. Due to the negative surface charge of the NBFs (the ζ-potential of NBFs is −37 mV at pH 7.0), the membrane is able to simultaneously separate oil and dye from water in milliseconds (Fig. 6A, Movie S8†).[15] By refeeding the membrane with oil/dyed-water several times the oil and dye (4 ppm) will be rejected and adsorbed by NBFs, respectively, and colorless water is obtained. The obtained adsorption capacity of the NBFs towards MB was 67 mg g^{-1}. Additionally, Fig. 6B shows the UV-visible spectra of the feed and filtered water solutions, in which the mother solution of MB (4 ppm) shows an absorption peak at 665 nm while this peak in the filtered water is completely omitted, proving the successful separation of the dye from the oil/water mixture.

We found out that when dropping a water droplet (2 μL) on the powder bed of the NBFs in air the water droplet is coated and stabilized with NBF particles after 3–4 seconds and an encapsulated water droplet is obtained that does not diffuse through the NBF powder (Fig. 7A, Movie S9†).[26–28] When we prepare a pellet bed from the NBF powder such behavior will not occur and water droplets penetrate through the NBF bed within milliseconds (Fig. 7A). In fact, the powder bed surface was wetted immediately by penetration of the water droplets and due to the capillary and viscous forces the wetted NBF particles start to move up around the water droplet, during which agitation of the NBF powder accelerates the process of particle aggregation into clusters (schematic in the inset in Fig. 7A). The water molecules bind the NBFs together as a bridge while water molecules cannot diffuse and approach poorly wetted NBFs; therefore water droplets were encapsulated by the shells of NBFs as a liquid marble and stabilized without leaking fluid.[56] To the best of our knowledge, this is the first report of preparing a marble droplet with a bio-originated, superamphiphilic material (*i.e.*, previous reported liquid marbles were prepared with either hydrophilic or hydrophobic materials).[25,29]

Furthermore, by dropping various volumes of water droplets from 10 to 80 μL on the powder bed of the NBFs, spherical water droplets are prepared where the contact angles of all the marble droplets were above 160° (Fig. 7B), while marble droplets with volumes larger than 80 μL showed slight distortions from the spherical shape due to the gravity and flexible puddle-like structure of the prepared marble droplets.[57] This implies that the combination of superamphiphilic, uniform, unbranched, and light weight properties of the NBFs, in air, is essential for generation of liquid marbles. Therefore, we studied these unique properties of the NBFs in more detail. As shown by the typical digital photographs in Fig. 7C, the liquid marbles were created simply by pouring a droplet of water or rolling water droplets on a powder bed of NBFs, and the NBFs spontaneously self-oriented due to the capillary forces and acted like shells and eventually more NBFs became attached on the surface of the liquid marble to prepare NBF multilayers and stabilize the water droplet at the water/air interface to encapsulate the core of the water droplet and prevent the water droplets from wetting their environment owing to their super hydrophilicity in air.[58,59] Fig. 7C shows a digital photograph of four liquid marbles prepared with a diameter of about 2.5 mm, which could be rolled freely by simply shaking a glass dish (Movie S10†). The weight ratio of the NBF shell and the core of the inner water droplet was about 1 : 10.

Another remarkable application of NBFs is the ability of NBF-based liquid marbles to be used as miniature adsorbent reactors towards the adsorption of encapsulated and trapped aqueous MB. 7 mL dyed-liquid marbles containing a 5 ppm MB solution are synthesized (Fig. 7D, Movie S11†).[57] Then the dyed-liquid marbles are ruptured at a pre-determined reaction time

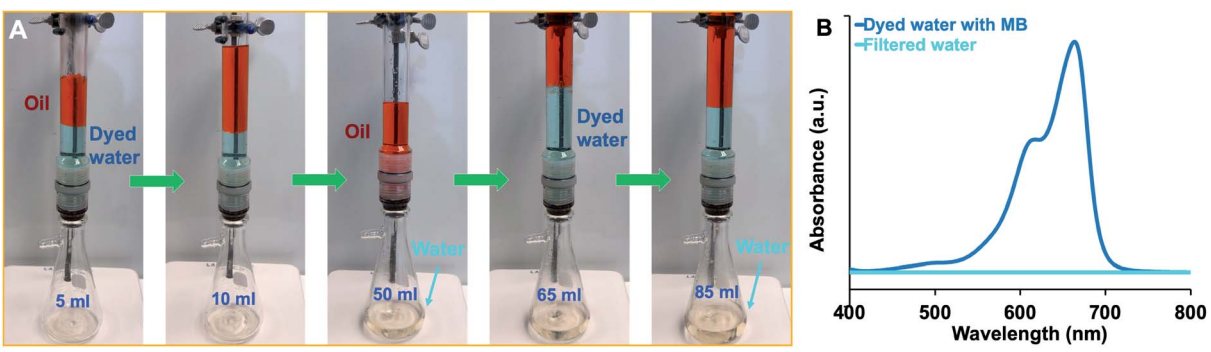

Fig. 6 (A) Photographs demonstrating the simultaneous oil/dye/water separation process using the NBF membrane (for clarity, the hexane oil phase was dyed red and the water phase contained MB dye). (B) The UV-vis spectra of the MB dyed water before and after the filtration process.

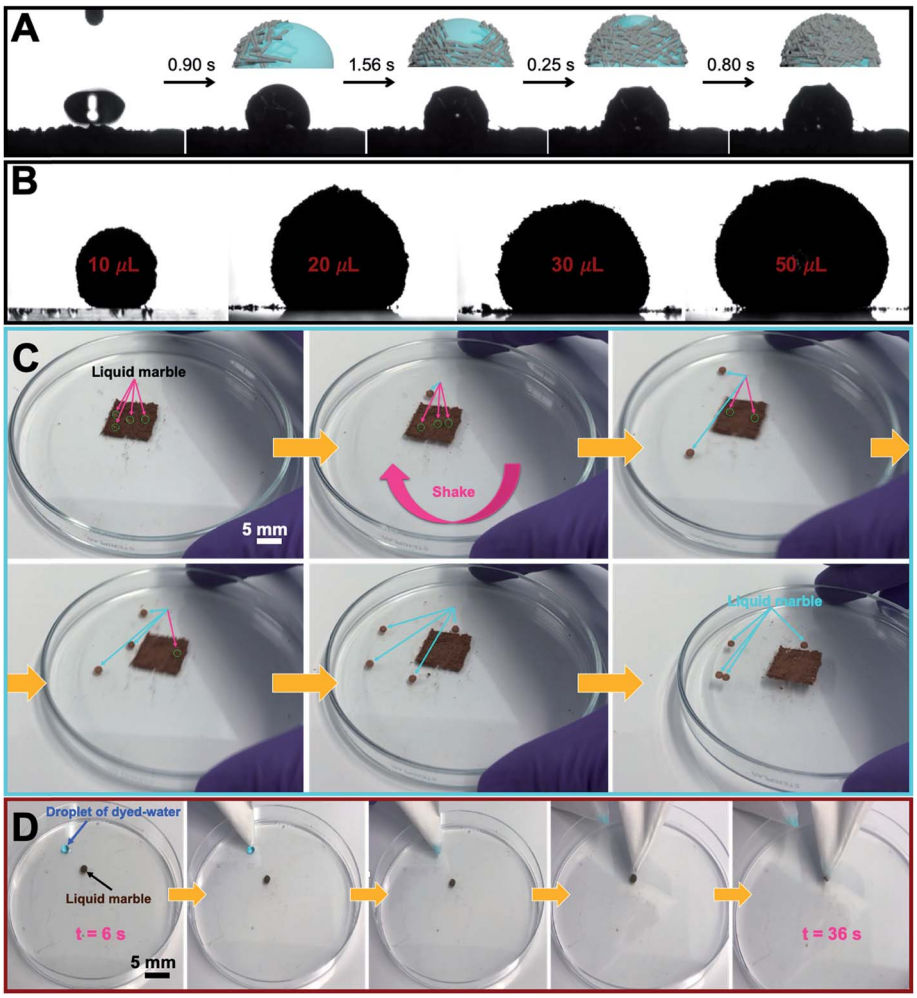

Fig. 7 (A) Sequential images of liquid marble preparation by spontaneous migration of NBFs to the water–air interface, which then encapsulate the water, (B) NBF-based liquid marbles prepared by encapsulation of water volumes ranging from 10 to 50 μL, (C) preparation of a liquid marble by rolling a water droplet on NBF powder which then became perfectly non-wetting when transferred on a glass Petri dish, and (D) snapshots indicating the color alteration of an aqueous methylene blue droplet without and in a NBF-based marble liquid after 36 seconds.

and the encapsulated MB solutions are gathered, and the color intensity of the MB solution after 36 seconds is visibly decreased and it turns colorless after 45 seconds, meaning that more than 99% of the MB was removed. Indeed, our proposed system benefits from the superior adsorption ability of NBFs, large surface area-to-volume ratios of NBFs, and their ability to generate low-cost, bio-originated and mechanically stable liquid marble shells having proper and potent interactions with contaminated water droplets. However, the obtained results indicated that NBFs could encapsulate 123 μL of water when the particle size of the NBFs is around 50 μm (Fig. S6,† Movie S12†). Indeed, a larger particle size showed higher adsorption energy and packing density on the surface of water droplets; therefore it would need a larger force to detach and disorder particles of NBFs, which meanwhile act as a physical barrier to water evaporation from the water surface to rupture the obtained large marble liquid.[59]

Water stress is a critical problem for plant growth in dry and arid weather and soils.[60] Therefore, based on the properties of the NBFs for encapsulation of high volume water droplets we set up an experiment to demonstrate the concept that NBFs are able to retain the humidity and water of soil in dry situations and release it slowly based on the need of the plant when they are added on the surface of soil or mixed with soil in comparison with pristine soil (see the ESI†).[61] For treatments with T1 and T2 after 20 days there are no signs of growing lentils while for treatments with T3 and T4 the growth of lentils was profuse when NBFs were added to the same amount of soil or mixed with the soil (Fig. S7†). By measuring the height of lentil plants for treatments with T3 (57 mm) and T4 (73 mm) and comparing with that for treatment with T1 (1.6 mm), it can be observed that the lentils in T3 and T4 grow 37 and 49 times higher, respectively. The height of the root for T3 and T4 reached 12 mm and 21 mm, respectively, which are 11 and 20 times higher compared to when only soil is used as the treatment. It is very evident that the presence of NBFs mixed with soil significantly increased the growth of lentils in arid situations by retaining the humidity and water and acting as a physical barrier to water evaporation around the lentil seeds and keeping them alive.[56]

4. Conclusion

We present a low-cost, green NBF membrane made from biomass using a simple, one-pot reaction without the use of any toxic reagent or solvent, or any specialized equipment. The resulting material demonstrated excellent separation capability for different stabilized, oily wastewater emulsions, as well as being able to simultaneously and rapidly separate dye from the oil/water mixture by gravity. Additionally, for the first time we prepared a liquid marble as a miniature reactor using a bio-originated superamphiphilic material instead of commonly used hydrophilic or superhydrophobic materials to remove dye from wastewater. As an added functionality, we demonstrated the ability of the NBF material to encapsulate a high volume water droplet (120 μL), allowing it to be used a soil additive for enhanced water retention, enabling us to grow a lentil plant under arid conditions. This work provides a low-cost sustainable material for the smart separation of stabilized emulsions in addition to its other multifunctional uses, suggesting its great potential for future applications in other fields.

Conflicts of interest

There are no conflicts to declare.

Acknowledgements

We thank the Cornell Center for Materials Research (CCMR) for the use of their facilities. CCMR facilities are supported by the National Science Foundation under award number DMR-1719875.

References

1 D. S. Sholl and R. P. Lively, *Nature*, 2016, **532**, 435–437.
2 M. Tao, L. Xue, F. Liu and L. Jiang, *Adv. Mater.*, 2014, **26**, 2943–2948.
3 W. Zhang, N. Liu, Y. Cao, Y. Chen, L. Xu, X. Lin and L. Feng, *Adv. Mater.*, 2015, **27**, 7349–7355.
4 J. R. Werber, C. O. Osuji and M. Elimelech, *Nat. Rev. Mater.*, 2016, **1**, 16018.
5 Z. Zhu, S. Zheng, S. Peng, Y. Zhao and Y. Tian, *Adv. Mater.*, 2017, **29**, 1703120.
6 Z. Chu, Y. Feng and S. Seeger, *Angew. Chem., Int. Ed.*, 2015, **54**, 2328–2338.
7 X. Yao, Y. Song and L. Jiang, *Adv. Mater.*, 2011, **23**, 719–734.
8 L. Wen, Y. Tian and L. Jiang, *Angew. Chem., Int. Ed.*, 2015, **54**, 3387–3399.
9 F. Li, Z. Wang, S. Huang, Y. Pan and X. Zhao, *Adv. Funct. Mater.*, 2018, **28**, 1706867.
10 F. Zhang, W. B. Zhang, Z. Shi, D. Wang, J. Jin and L. Jiang, *Adv. Mater.*, 2013, **25**, 4192–4198.
11 M. Liu, Y. Hou, J. Li and Z. Guo, *Langmuir*, 2017, **33**, 3702–3710.
12 P. Zhou, J. Li, W. Yang, L. Zhu and H. Tang, *Langmuir*, 2018, **34**, 2841–2848.
13 Y. Dong, C. Huang and X.-Y. Yang, *Chem. Eng. J.*, 2019, **361**, 322–328.
14 Y. Long, Y. Shen, H. Tian, Y. Yang, H. Feng and J. Li, *J. Membr. Sci.*, 2018, **565**, 85–94.
15 X. Wang, M. Li, Y. Shen, Y. Yang, H. Feng and J. Li, *Green Chem.*, 2019, **21**, 3190–3199.
16 P. Zhang, S. Wang, S. Wang and L. Jiang, *Small*, 2015, **11**, 1939–1946.
17 W. Zhang, N. Liu, Q. Zhang, R. Qu, Y. Liu, X. Li, Y. Wei, L. Feng and L. Jiang, *Angew. Chem., Int. Ed.*, 2018, **57**, 5740–5745.
18 G. Kwon, A. K. Kota, Y. Li, A. Sohani, J. M. Mabry and A. Tuteja, *Adv. Mater.*, 2012, **24**, 3666–3671.
19 Z. Lei, G. Zhang, Y. Deng and C. Wang, *ACS Appl. Mater. Interfaces*, 2017, **9**, 8967–8974.
20 H. Kang, Y. Liu, H. Lai, X. Yu, Z. Cheng and L. Jiang, *ACS Nano*, 2018, **12**, 1074–1082.
21 G. Cao, Y. Wang, C. Wang and S.-H. Ho, *J. Mater. Chem. A*, 2019, **7**, 11305–11313.
22 C. Beres, G. N. S. Costa, I. Cabezudo, N. K. da Silva-James, A. S. C. Teles, A. P. G. Cruz, C. Mellinger-Silva, R. V. Tonon, L. M. C. Cabral and S. P. Freitas, *Waste Manag.*, 2017, **68**, 581–594.
23 R. Devesa-Rey, X. Vecino, J. L. Varela-Alende, M. T. Barral, J. M. Cruz and A. B. Moldes, *Waste Manag.*, 2011, **31**, 2327–2335.
24 G. A. Martinez, S. Rebecchi, D. Decorti, J. M. B. Domingos, A. Natolino, D. Del Rio, L. Bertin, C. Da Porto and F. Fava, *Green Chem.*, 2016, **18**, 261–270.
25 E. Bormashenko, R. Pogreb, A. Musin, R. Balter, G. Whyman and D. Aurbach, *Powder Technol.*, 2010, **203**, 529–533.
26 Z. Liu, T. Yang, Y. Huang, Y. Liu, L. Chen, L. Deng, H. C. Shum and T. Kong, *Adv. Funct. Mater.*, 2019, **29**, 1901101.
27 Y. Wang, K. Ma and J. H. Xin, *Adv. Funct. Mater.*, 2018, **28**, 1705128.
28 X. Rong, R. Ettelaie, S. V. Lishchuk, H. Cheng, N. Zhao, F. Xiao, F. Cheng and H. Yang, *Nat. Commun.*, 2019, **10**, 1854.
29 P. Aussillous and D. Quéré, *Nature*, 2001, **411**, 924–927.
30 M. Soleymanzadeh, M. Arshadi, J. W. L. Salvacion and F. SalimiVahid, *Chem. Eng. Res. Des.*, 2015, **93**, 696–709.
31 H. Eskandarloo, M. Arshadi, M. Azizi, M. Enayati and A. Abbaspourrad, *ACS Sustainable Chem. Eng.*, 2019, **7**, 3895–3908.
32 M. Arshadi, J. E. Gholtash, H. Zandi and S. Foroughifard, *RSC Adv.*, 2015, **5**, 43290–43302.
33 M. Arshadi, S. Foroughifard, J. Etemad Gholtash and A. Abbaspourrad, *J. Colloid Interface Sci.*, 2015, **452**, 69–77.
34 C. Tan, M. Arshadi, M. C. Lee, M. Godec, M. Azizi, B. Yan, H. Eskandarloo, T. W. Deisenroth, R. H. Darji, T. V. Pho and A. Abbaspourrad, *ACS Nano*, 2019, **13**(8), 9016–9027.
35 C. Tan, S. Pajoumshariati, M. Arshadi and A. Abbaspourrad, *Chem. Commun.*, 2019, **55**, 1225–1228.
36 J. Nogales-Bueno, B. Baca-Bocanegra, A. Rooney, J. M. Hernández-Hierro, H. J. Byrne and F. J. Heredia, *Food Chem.*, 2017, **232**, 602–609.

37 M. Fasoli, R. Dell'Anna, S. Dal Santo, R. Balestrini, A. Sanson, M. Pezzotti, F. Monti and S. Zenoni, *Plant Cell Physiol.*, 2016, **57**, 1332–1349.
38 M. Li, L.-j. Wang, D. Li, Y.-L. Cheng and B. Adhikari, *Carbohydr. Polym.*, 2014, **102**, 136–143.
39 M. Thiripura Sundari and A. Ramesh, *Carbohydr. Polym.*, 2012, **87**, 1701–1705.
40 A. Mtibe, L. Z. Linganiso, A. P. Mathew, K. Oksman, M. J. John and R. D. Anandjiwala, *Carbohydr. Polym.*, 2015, **118**, 1–8.
41 P. Tharra and B. Baire, *Chem. Commun.*, 2016, **52**, 14290–14293.
42 P. Lu and Y.-L. Hsieh, *Carbohydr. Polym.*, 2010, **82**, 329–336.
43 Y. Shimazaki, Y. Miyazaki, Y. Takezawa, M. Nogi, K. Abe, S. Ifuku and H. Yano, *Biomacromolecules*, 2007, **8**, 2976–2978.
44 T. Sun, L. Feng, X. Gao and L. Jiang, *Acc. Chem. Res.*, 2005, **38**, 644–652.
45 M. Liu, Y. Zheng, J. Zhai and L. Jiang, *Acc. Chem. Res.*, 2010, **43**, 368–377.
46 Y. Wu, J. Feng, H. Gao, X. Feng and L. Jiang, *Adv. Mater.*, 2019, **31**, 1800718.
47 H.-C. Yang, Y. Xie, H. Chan, B. Narayanan, L. Chen, R. Z. Waldman, S. K. R. S. Sankaranarayanan, J. W. Elam and S. B. Darling, *ACS Nano*, 2018, **12**, 8678–8685.
48 L. Lin, M. Liu, L. Chen, P. Chen, J. Ma, D. Han and L. Jiang, *Adv. Mater.*, 2010, **22**, 4826–4830.
49 J. Li, C. Xu, C. Guo, H. Tian, F. Zha and L. Guo, *J. Mater. Chem. A*, 2018, **6**, 223–230.
50 S. Yuan, J. Zhu, Y. Li, Y. Zhao, J. Li, P. Van Puyvelde and B. Van der Bruggen, *J. Mater. Chem. A*, 2019, **7**, 2723–2729.
51 P. d. calculation, https://www.powderprocess.net/Pneumatic_Transport/Pressure_Drop_Calculation_Dilute_Phase.html.
52 W. Lv, Q. Mei, J. Xiao, M. Du and Q. Zheng, *Adv. Funct. Mater.*, 2017, **27**, 1704293.
53 R. Hönes and J. Rühe, *Langmuir*, 2018, **34**, 5342–5351.
54 Z. Xue, S. Wang, L. Lin, L. Chen, M. Liu, L. Feng and L. Jiang, *Adv. Mater.*, 2011, **23**, 4270–4273.
55 C. Lee and S. Baik, *Carbon*, 2010, **48**, 2192–2197.
56 C. P. Whitby, X. Bian and R. Sedev, *Colloids Surf., A*, 2013, **436**, 639–646.
57 Y.-E. Miao, H. K. Lee, W. S. Chew, I. Y. Phang, T. Liu and X. Y. Ling, *Chem. Commun.*, 2014, **50**, 5923–5926.
58 D. Wang, L. Zhu, J.-F. Chen and L. Dai, *Angew. Chem., Int. Ed.*, 2016, **55**, 10795–10799.
59 Z. Liu, Y. Zhang, C. Chen, T. Yang, J. Wang, L. Guo, P. Liu and T. Kong, *Small*, 2019, **15**, 1804549.
60 N. Raddadi, L. Giacomucci, R. Marasco, D. Daffonchio, A. Cherif and F. Fava, *Microb. Cell Fact.*, 2018, **17**, 83.
61 M. Dandan and H. Y. Erbil, *Langmuir*, 2009, **25**, 8362–8367.